Journal of Anatomy

J. Anat. (2013) **223**, pp462–473 doi: 10.1111/joa.12102

Three-dimensional skeletal kinematics of the shoulder girdle and forelimb in walking *Alligator*

David B. Baier[1] and Stephen M. Gatesy[2]

[1]*Department of Biology, Providence College, Providence, RI, USA*
[2]*Department of Ecology and Evolutionary Biology, Brown University, Providence, RI, USA*

Abstract

Crocodylians occupy a key phylogenetic position for investigations of archosaur locomotor evolution. Compared to the well-studied hindlimb, relatively little is known about the skeletal movements and mechanics of the forelimb. In this study, we employed manual markerless XROMM (X-ray Reconstruction Of Moving Morphology) to measure detailed 3-D kinematics of the shoulder girdle and forelimb bones of American alligators (*Alligator mississippiensis*) walking on a treadmill. Digital models of the interclavicle, scapulocoracoid, humerus, radius and ulna were created using a 3-D laser scanner. Models were articulated and aligned to simultaneously recorded frames of fluoroscopic and standard light video to reconstruct and measure joint motion. Joint coordinate systems were established for the coracosternal, glenohumeral and elbow joints. Our analysis revealed that the limb joints only account for about half of fore/aft limb excursion; the remaining excursion results from shoulder girdle movements and lateral bending of the vertebral column. Considerable motion of each scapulocoracoid relative to the vertebral column is consistent with coracosternal mobility. The hemisellar design of the glenohumeral joint permits some additional translation, or sliding in the fore-aft plane, but this movement does not have much of an effect on the distal excursion of the bone.
Key words: alligator; coracoids; kinematics; shoulder; treadmill.

Introduction

Modern crocodylians and birds are the only surviving members of Archosauria, a ~250 million-year-old clade including dinosaurs, pterosaurs and other less widely known members (Nesbitt, 2011). The archosaurian radiation gave rise to several novel locomotor adaptations, such as diverse postures, bipedality, reversions to quadrupedality and independent origins of powered flight (e.g. Hutchinson, 2006). Given their phylogenetic position, living crocodylians help anchor the extant phylogenetic bracket for extinct archosaurs (Witmer, 1995; Allen et al. 2010). For example, efforts to reconstruct aspects of limb anatomy and function in Mesozoic dinosaurs and the origin of avian flight rely heavily on crocodylian morphology (Nicholls & Russell, 1985; Jenkins, 1993; Paul & Christiansen, 2000; Jasinoski et al. 2006).

The majority of investigations into crocodylian terrestrial locomotion concentrate on the hindlimb (Gatesy, 1991, 1997; Blob & Biewener, 1999, 2001; Reilly & Blob, 2003; Reilly et al. 2005). Major advances have been made in clarifying crocodylian forelimb myology (Meers, 2003; Allen et al. 2010), ground reaction forces (Willey et al. 2004) and joint ranges of motion based on manipulation of specimens post mortem (Jenkins, 1993; Hutson, 2012; Hutson & Hutson, 2012). However, there are currently no quantitative studies documenting skeletal kinematics of crocodylian forelimbs *in vivo*. Forelimb motion measured externally (e.g. Bakker, 1971) likely suffers from artifacts of overlying muscle and loose skin (Zatsiorsky, 1998; Leardini et al. 2005; Gatesy et al. 2010). Without direct skeletal visualization by X-ray imaging, long-axis rototation and subtle translations, particularly among elements of the pectoral girdle, are difficult to quantify accurately.

In the absence of high-resolution crocodylian kinematic data, many functional comparisons rely on a cineradiographic analysis of the terrestrial lepidosaur, *Varanus exanthematicus* (Jenkins & Goslow, 1983). However, living crocodylians exhibit a wider variety of gaits and postures than terrestrial lepidosaurs, including a continuum from bellycrawls to semi-erect postures, bounding and galloping (Cott, 1961; Zug, 1974; Gatesy, 1991; Reilly & Elias, 1998; Renous et al. 2002). Movements among deep elements of the shoulder girdle remain particularly elusive and have never been studied in crocodylians. Conflicting evidence of coracosternal movements in lepidosaurs has been

Correspondence
David B. Baier, Department of Biology, Providence College, Providence, RI 02918, USA. T: 401-865-2172; F: 401-865-1438; E: dbaier@providence.edu

Accepted for publication *5 August 2013*
Article published online *15 September 2013*

reported. In *Varanus*, Jenkins & Goslow (1983) found extensive coracosternal sliding, whereas Peterson (1984) suggested that terrestrial lizards like *Agama* maintain a fixed coracoid. Biplanar X-ray video reveals a highly mobile coracosternal joint in chameleons (Fischer et al. 2010), but the level of coracosternal movement in other saurians remains enigmatic.

Here, we merge X-ray video, standard light video and laser-scanned models of American alligator bones using the recently described method of Scientific Rotoscoping (Gatesy et al. 2010; Nyakatura & Fischer, 2010; Baier et al. 2013), also known as manual markerless XROMM (X-ray Reconstruction Of Moving Morphology; Brainerd et al. 2010), to yield detailed measures of joint and limb movements of the forelimb skeleton during the 'high-walk' for the first time.

Materials and methods

Animals and external markers

Over a period of several weeks, three American alligators (*Alligator mississippiensis*; Table 1) were trained to walk within a clear acrylic running box suspended above a motorized treadmill. Animals were housed and cared for under animal care committee monitoring at the Museum of Comparative Zoology, Harvard University. Alligator1 had no obvious musculoskeletal abnormalities. Alligator2 was missing three toes on the left forefoot. Alligator3 had a healed right humeral fracture. There were no obvious locomotor deficits associated with these skeletal anomalies.

Three radio-opaque markers (small metal washers and nuts) were attached to osteoderms at the level of the shoulder girdle using cyanoacrylate adhesive. The first was positioned on the midline between dorsal scutes just posterior to the neck, the second between dorsal midline scutes two rows caudal to the first, and the third on a lateral scute in the same region (Fig. 1). Markers did not interfere with vertebral or forelimb motion. Translations and rotations of this marker triad allowed tracking of the underlying group of vertebrae, to which the osteoderms are firmly attached.

Manual markerless XROMM

General methodology

Manual markerless XROMM (Gatesy et al. 2010) was used to simultaneously animate and quantify 3-D bone movement based on X-ray and standard video. Briefly, elements of the experimental setup (components of the fluoroscopic imaging system, standard video camera and treadmill) were first recreated as a 3-D scene using animation software (Maya 2010, Autodesk). Virtual cameras were positioned and aimed to recreate the same perspectives as the actual X-ray beam and standard camera. Frames of distortion-corrected video were displayed on background planes for viewing through each virtual camera. Polygonal models of shoulder girdle and forelimb bones were then created from laser scans and articulated by virtual joints into a hierarchical, digital marionette. Finally, the skeletal puppet was posed by registering each bone model to match the X-ray and standard video background images. Rotation and translation values for the model's 18 degrees of freedom were saved over a sequence of frames, yielding high-resolution kinematic data and anatomically accurate animations.

Table 1 Summary data of Alligator specimens.

	Mass (kg)	Humeral length (cm)	Humeral head width (cm)	Coracoid base width (cm)	Strides analyzed
Alligator1	3.08	6.7	1.7	2.1	7
Alligator2	1.66	5.6	1.4	1.8	6
Alligator3	1.08	5.0	1.3	1.6	7

Video recording

X-ray images were recorded in either lateral or dorso-ventral projection. A Sony DCR-VX1000 digital handycam was attached to a Siemens cineradiographic apparatus (0.06 mm focal spot, 27.94 cm Sirecon image intensification system) to record from the image intensifier's output window. An S-video cable transferred video to a separate Sony TRV770 VCR for recording on Hi8 tape. A second camera (Sony DCR-TRV30) was configured to record standard (light) video orthogonal to the X-ray beam. Synchronization was achieved by flashing a small LED placed at the edge of each lens, which allowed identification of comparable frames.

Digital video was downloaded from the tapes to QuickTime clips using Premiere 6.5 (Adobe). The 30 frame per second clips were then de-interlaced and broken into jpeg image sequences at 60 fields per second using MayaFusion (Autodesk). Because motion was relatively slow, only half (30 fields per second) were analyzed. Only sequences in which animals maintained a relatively steady pace over several strides were chosen for rotoscoping.

Experimental setup

Maya (Autodesk) animation software was used to reconstruct the experimental setup in 3-D (Gatesy et al. 2010). Images of standardized grids were taken with both cameras. In Maya, grid images were projected on a plane. When looking at this plane through an orthogonal camera, the grids appear distorted due to non-linearities of the camera, lens and image intensifier (e.g. Dobbert, 2005). Using a model of a uniform reference grid as a template, control vertices were moved to scale and warp the spline-based plane until each grid image was squared.

Camera calibration began by placing virtual cameras at the approximate locations based on laboratory measurements. Refinement of position and orientation was done using images of calibration objects of various shape and size (primarily Lego blocks) that were placed at known coordinates within the field of view of both cameras. Then, the calibration objects were modeled in Maya and placed at the same coordinates in the virtual scene. If the virtual cameras and image planes are accurately placed, oriented and scaled, the calibration object models should line up with the video images. Minor adjustments of initial measured camera positions were made to fine tune the position and orientation of the cameras relative to the calibration objects (Gatesy et al. 2010). Once completed, the 3-D position and orientation of objects in the field of view of both cameras could be reconstructed and quantified by registering models to their recorded images (Fig. 1).

The shoulder girdles and upper arm bones overlap considerably in lateral X-ray views, making bone orientation ambiguous in some of the phases of the stride sequences. Therefore, only dorsoventral X-ray sequences, in conjunction with orthogonal lateral standard

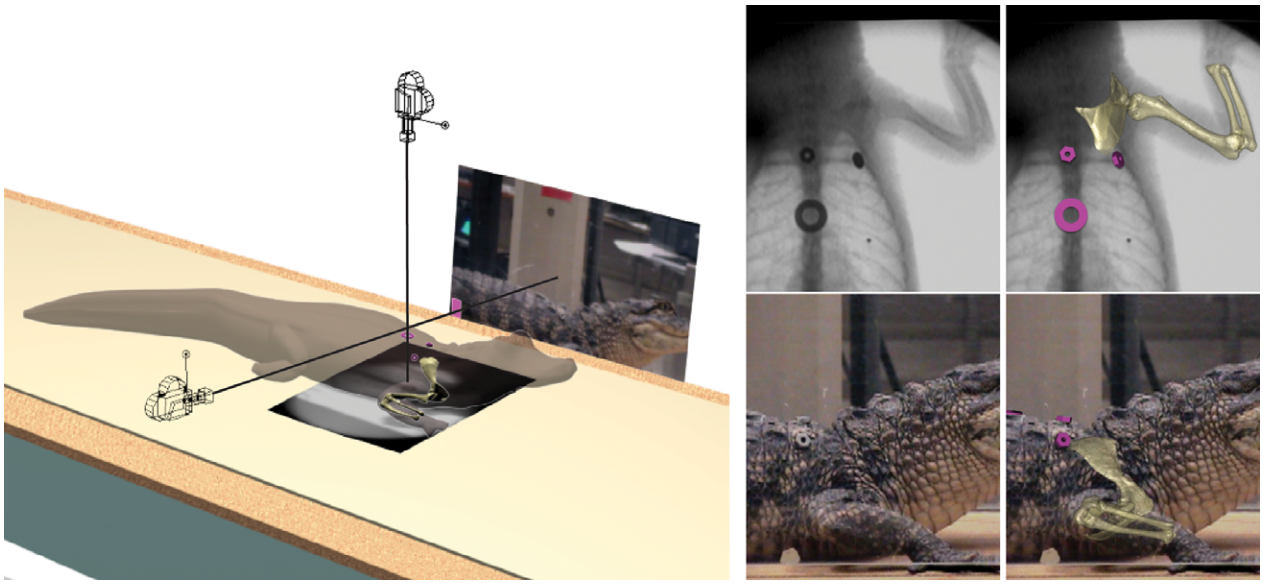

Fig. 1 Maya setup for dorsoventral X-rays of treadmill walking. Virtual cameras and background planes reproduce X-ray source and standard video perspectives (camera icons shown closer to subject for clarity). Models of body markers (fuscia) and skeletal elements (gold) are registered in 3-D for individual frames.

video, were used for measuring joint motion. Lateral X-ray views were checked to verify that reconstructed movements were similar from both perspectives.

Three-dimensional alligator bone models

Alligator1 was the best walker (most consecutive strides for the most runs at a constant velocity) and therefore was used for the computer-generated skeletal model. Three-dimensional laser scans (ShapeGrabber -SG100) produced polygonal models of the bones of the right forelimb and shoulder girdle with intact articular cartilages. Scans were made immediately after dissection, and bones and cartilage were spray painted white to minimize artifacts from the scanner. Files for individual bones were then imported into Maya.

Maya – virtual skeleton setup

Virtual bones for Alligator1 were articulated by still X-rays and dissected specimens. By parenting models to a hierarchical chain of pivot points (a 'kinematic skeleton' in Maya), their positions and orientations can be controlled by virtual joints (Fig. 2; Gatesy et al. 2010). The top joint in the hierarchy moves all joints below, so that if the whole body moves, the shoulder girdles and the forelimbs move as well. By measuring each joint within this nested hierarchy, each degree of freedom can be studied independently.

We initially assumed that each joint affecting forelimb motion had six degrees of freedom (three rotations and three translations). Pivots were initially placed at the center of each joint with three rotational degrees of freedom and were oriented with respect to the anatomy of the proximal joint surface. The 'zero' pose was based on the anatomy of the distal element relative to the joint coordinate system. Translations were constrained to an arc along the primary axis of the joint surface. The curvature of this arc can be described as a segment of a circle with a radius that most closely matches the curvature of the joint surface.

Girdle and limb motion was measured at four points: (i) scute markers relative to a lab coordinate system; (ii) coracoid relative to the scute markers; (iii) humerus relative to the scapulocoracoid; and (iv) ulna/radius relative to the humerus. Wrist motion was not quantified in this study.

Coordinate systems

Each coordinate system (Fig. 2) follows an XYZ (red, green and then blue) rotation order in Maya. In our joint coordinate systems, the Z (blue) axis remains fixed to the proximal element, the X (red) axis orients down the long-axis of the distal element, and the Y (green axis) remains perpendicular to both Z and X (Grood & Suntay, 1983). It is important to note that this order of rotation dictates that rotations about the blue axis affect the orientation of both the green and red axis, the green axis affects the orientation of the red axis, and the red axis does not affect the orientation of the blue or green. The right-hand rule can be used in each instance to interpret positive and negative direction of rotations (where the thumb of the right hand points in the direction of the arrowhead and the curvature of the fingers indicates the positive rotation about the axis).

(1) Vertebral coordinate system

Rotations (Z = yaw, Y = pitch and X = roll) and XYZ translations of the body in the region of the pectoral girdle were measured by registering (rotoscoping) the cluster of three skin marker models to their X-ray and light video images. Small inter-scute movements were detectable between the dorsal markers, but intervertebral kinematics were not quantified. This pivot was centered on the anterior scute marker (Fig. 2; joint1). Zero yaw, pitch and roll of the body were determined from video of Alligator1 when lying still on its belly. At 0 ° yaw, the dorsal midline markers are parallel with the direction of travel on the treadmill. At 0 ° pitch, the posterior midline marker is slightly higher than the anterior marker, but the vertebral column in the region of the pectoral girdle is horizontal.

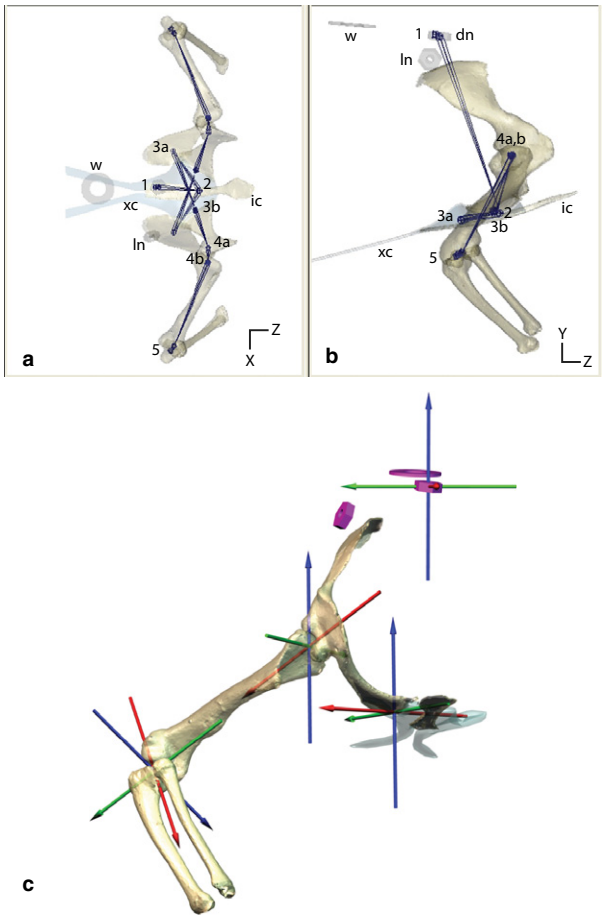

Fig. 2 Joint control and coordinate systems. (a and b) Maya 'joints' (dots) connected by Maya 'bones' (lines) underlie the polygonal models and control each degree of freedom. The hierarchy is controlled in the following order: (1) whole-body rotations and translations; (2) sternal motions relative to the vertebral column; (3a) controls glenoid non-linear translation; (3b) coracoid rotations; (4a) humeral non-linear translation; (4b) humeral rotations; (5) elbow rotations. dn, dorsal nut; ic, interclavicle; ln, lateral nut; w, washer; xc, xiphisternal cartilage. (c) Vertebral and joint coordinate systems used to measure skeletal movements.

At 0 ° roll, the lateral axis passing through both shoulders is horizontal. If the head was to remain fixed relative to the vertebral column, rotations about these axes yield the following: positive yaw (Fig. 2c; blue) = nose to the left; positive pitch = nose up (Fig. 2c; green); positive roll = left side raised above the right (Fig. 2c; red).

(2) Coracosternal joint

The coracosternal pivot was placed at the center of the proximal coracoid joint surface. Protraction and retraction (Fig. 2c; blue) is a rotation about the vertical axis perpendicular to the long-axis of the proximal coracoid. Abduction/adduction (Fig. 2c; green) occurs about the long-axis of the joint and pitch occurs about the horizontal axis perpendicular to the long-axis of the joint (Fig. 2c; red).

An additional sliding component permits the coracoid to translate along the curvature of the joint without rotating (Fig. 2a,b). The zero position was based on a still X-ray of Alligator1.

(3) Glenohumeral joint

The three rotational degrees of freedom (protraction/retraction, abduction/adduction and pronation/supination) are oriented relative to the glenoid articular surface. At 0 ° protraction the long-axis of the humerus points laterally, perpendicular to the vertebral column. At 0 ° abduction, the humerus is parallel to the ground. At 0° pronation, the deltopectoral crest points ventrally and the distal condyles parallel to the vertebral column.

The pivot of the glenohumeral joint is in the center of the humeral head. Protraction/retraction occurs about the long-axis of the glenoid. Abduction/adduction occurs about the short axis in the plane of the convexity of the glenoid and pronation/supination about the long-axis of the humerus (aiming from the center of the humeral head to the center of the distal condyles). Our orientations follow Jenkins (1993), but note that other shoulder movement descriptions have been used (Hutson & Hutson, 2012).

(4) Elbow joint

The flexion/extension and abduction/adduction axes were oriented relative to the distal humeral condyles, but the axes were located on the intercondylar eminence on the ulnar articular cartilage (Fig. 6a,b). At 0° extension and abduction/adduction, the ulna's long-axis (passing through both the proximal and distal joint surfaces) aligns with the long-axis of the humerus. At 0° long-axis rotation, the curvature of the ulna is in a plane perpendicular to the long-axis of the humerus. Abduction is positive rotation about the green axis (lateral deviation of the ulna relative to the humerus). Long-axis rotation occurs about the long-axis of the ulna.

Animation

The virtual skeleton was registered to video sequences by aligning bone models to their dorsoventral X-ray shadows, assisted by height information from the lateral light video. The rotoscoping process is iterative, requiring numerous passes through each sequence. No internal bone markers were needed; the entire shape of the bone guided placement.

Walking speed was calculated by averaging the velocity of the third toe during the stance phase over several strides.

Maya – scaling between animals

The virtual skeleton from Alligator1 was scaled to grossly match the other two alligators based on humeral length, and then tailored based on still X-ray and video sequences. No adjustments were made to the underlying kinematic skeleton to ensure that measurements between animals were comparable. The position and orientation of the body markers were adjusted specifically for their unique attachments on each animal.

Results

General kinematics

All strides analyzed in this study were from 'high-walk' sequences (Cott, 1961; Gatesy, 1991; Willey et al. 2004) in which the humerus was adducted an average of -29.4 ± 5.8 °. Walking velocities ranged from 0.16 to 0.38 m s^{-1}. The larger individual averaged 0.35 ± 0.04 m s^{-1} and the two smaller alligators averaged 0.18 ± 0.01 m s^{-1}. The average

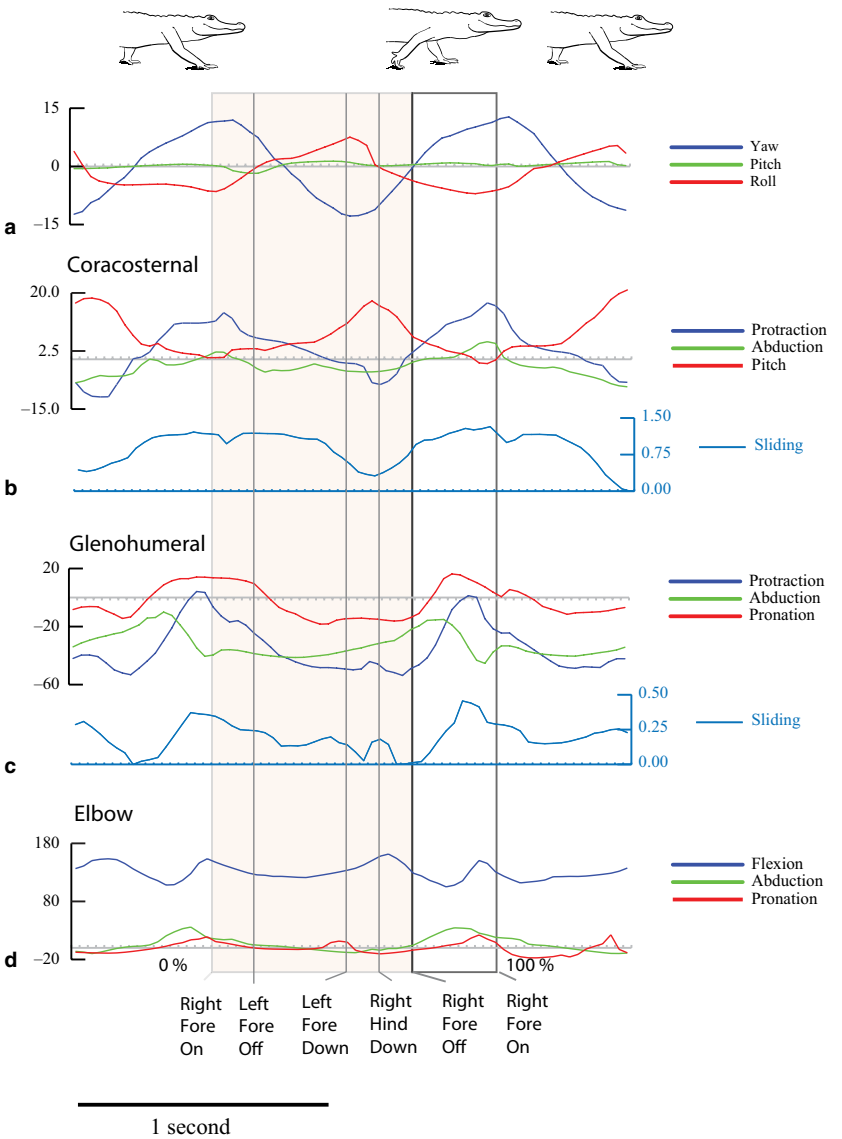

Fig. 3 Two representative strides for Alligator1 walking at 0.31 m s^{-1} with stride events marked. The shaded area is stance phase. Colors match Fig. 2 joint coordinate systems. (a) Yaw, pitch and roll of the dorsal scute markers in the shoulder region. Positive yaw is to the left; negative yaw is to the right. Positive pitch is nose up; negative pitch is nose down. Positive roll is to the left; negative roll is to the right. The scute marker movements are a proxy for the vertebral reference frame. (b) Coracosternal movements. Protraction is positive and retraction is negative (blue). Adduction is positive and abduction is negative. Positive pitch moves the dorsal end of the scapula posteriorly and negative pitch moves the dorsal scapula anteriorly. Cranial sliding is positive and caudal sliding is negative. (c) Glenohumeral protraction is positive and retraction is negative. Abduction of the humerus above the horizontal plane is positive and adduction below the horizontal plane is negative. Pronation is negative and supination is positive. Cranial sliding is positive and caudal sliding is negative. (d) Elbow extension is positive. Flexion refers to a decreasing angle of movement. Abduction is a lateral deviation relative to the humeral condyles and is positive. Adduction is a medial deviation relative to the humeral condyles and is negative. Pronation is negative and supination is positive.

stride frequency was 1.2 ± 0.2 Hz and duty factor averaged 0.66 ± 0.06.

We defined a stride in reference to the right forelimb from toe down (0%) to subsequent toe down (100%). The digits sequentially lifted throughout the final portion of stance, beginning with digit V at 41.26 ± 9.95% of the stride. Prior to liftoff, the remaining digits were dorsiflexed and the wrist moved vertically relative to the tread. Swing phase began (66.0 ± 6.1%) with a rapid plantar flexion of distal joints of digits II and III. Initially, the hand dropped and its dorsal surface typically dragged on the substrate before swinging upward and forward in preparation for the next stride. The right pes occasionally contacted the right manus at the end of stance. The left manus lifted during the first half of right stance and landed again near the right stance/swing transition.

Movement of the thorax in the shoulder region

During the high-walk, the anterior thorax increased 12 ± 6% about the average vertebral height. Scute markers increased in height until approximately mid-stance and then dropped through late stance. Lateral translations were less consistent, but the body typically moved towards the stance limb at the beginning of stance, then away from the stance limb through midstance, and towards the stance limb again through swing phase.

Yaw pattern was approximately sinusoidal, reaching extremes (about 10 °) away from the stance limb at the beginning of stance phase (Fig. 3a). Pitch was relatively small (range 5 ± 2 °). The pattern of roll was more variable, particularly between the large and small animals, but the range (10 ± 3 °) was similar for all strides (Table 2).

Table 2 Summary of body and joint motion.

	Mean	± SD
Body rotations		
Yaw range	20.0	5.6
Pitch range	5.2	2.2
Roll range	10.0	3.4
Coracoid		
Translation (cm)	0.9	0.2
Translation (% joint length)	50.8%	14.0%
Protraction maximum	17.1	6.2
Retraction minimum	−10.4	3.6
Abduction maximum	6.5	4.6
Adduction minimum	−4.4	3.6
Spin maximum	17.5	4.1
Spin minimum	−4.8	4.4
Humerus		
Translation (cm)	0.3	0.1
Translation (% joint length)	18.6%	7.6%
Protraction maximum	−5.0	17.7
Retraction minimum	−57.0	7.7
Abduction maximum	−4.6	11.6
Adduction minimum	−45.7	9.1
Supination maximum	27.2	13.1
Pronation minimum	−17.9	8.1
Elbow		
Extension maximum	159.3	6.2
Flexion minimum	85.9	21.7
Abduction maximum	29.4	9.1
Adduction minimum	−11.6	6.6
Supination maximum	8.8	10.0
Pronation minimum	−21.8	5.7

Coracosternal joint

The scapulae are tightly synostosed with the coracoids to form scapulocoracoids, which articulate with paired cartilaginous sterna on either side of a bony interclavicle. The anterolateral sternal surfaces form a pair of articular grooves angled obliquely at about 15 ° relative to the sagittal plane (Fig. 4b). The proximal coracoid forms a tongue-shaped articular surface that rides along the shallow arc of the sternal groove. The cranial boundary of the sternal groove lies at the lateral margin of the interclavicle. The caudal sternal articular surface is open-ended; coracoid movement is limited by connective tissue at the margin of the joint. Tongue and groove articulations generally constrain motion to the plane of the groove, but the sternum's cartilaginous nature and mobile connective tissues allow additional flexibility.

Four degrees of freedom (three rotations and one sliding) were required to replicate the motion of the right coracoid relative to the vertebral markers as recorded by dorsoventral and lateral X-ray video (see Materials and methods).

At the beginning of stance, the proximal coracoid was near its cranial-most position with respect to the vertebral markers. During stance, the coracoid slid posteriorly an average of 51 ± 13% of proximal coracoid width. Simultaneously, the coracoid retracted, pitched to make the scapula more vertical, and abducted (Fig. 4) in such a way that the vertebral end of the scapula remained reasonably fixed relative to the body wall. These coordinated movements shifted the glenoid caudally and laterally, directing its face more posteriorly and its long-axis more vertically as stance phase progresses (Fig. 4).

For all four degrees of freedom, changes were tightly coupled with the period prior to the end of stance phase at ipsilateral hindlimb contact (Fig. 3). Hence, the coracoid began protracting (rotating) and sliding (translating) cranially before toe off during the brief period of triple support.

Glenohumeral joint

The glenohumeral joint is a hemi-sellar or half-saddle joint (Jenkins, 1993), in which the relatively large, ovoid humeral head articulates with a shallow, saddle-shaped glenoid. The glenoid cavity is bounded by a dorsal lip from the scapula and a ventral lip from the coracoid. The long-axis of the humeral head aligns along the convexity of

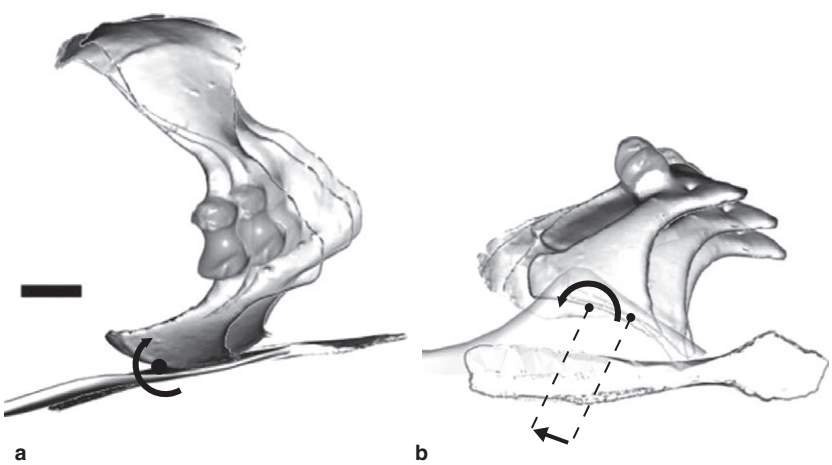

Fig. 4 Coracosternal joint motion during stance phase of a single stride. (a) In lateral view, pitching of the coracoid is apparent, the relatively fixed point near the dorsal margin of the scapula combined with sliding and retraction at the coracosternal joint reorients the glenoid during stance. (b) In ventral view, the large displacement of the coracoid results both from translation (0.8 cm in this stride) and rotation along the coracosternal groove.

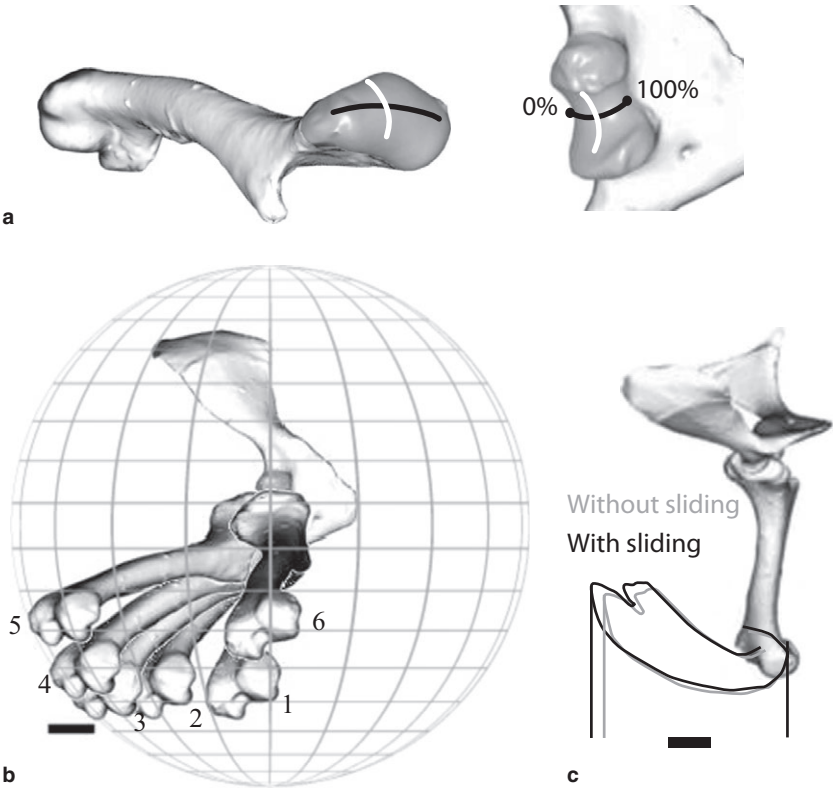

Fig. 5 Glenohumeral joint. (a) The long-axis convexity of the humeral head aligns along the short convexity of the glenoid (black line), and the short convexity of the humeral head aligns along the long-axis concavity of the glenoid (white line) forming a hemisellar arrangement. The open cranial and caudal margins of the joint allow an additional degree of freedom, translational sliding. (b) Typical path of the humerus during a single stride in lateral view after vertebral and coracosternal motions are factored out. 1 = beginning of stance phase; 6 = end of swing phase. (c) Translational sliding slightly increases the displacement of the elbow during a single representative stride.

the saddle, approximately craniocaudally (Fig. 5a). Along the short axis, the humeral head and glenoid are narrower cranially and wider caudally. The joint surfaces allow a wide range of movement, particularly protraction and retraction along the convexity of the glenoid. As with the coracosternal joint, translation of the humeral head was measured as a single degree of freedom by following an arc conforming to the smaller, convex radius of the middle of the glenoid.

The humerus retracted during stance and protracted during swing through a range of $52 \pm 12°$ – beginning stance at $-20°$, ending stance at $-57°$, protracting through swing phase to $-5°$, and then beginning to retract prior to touchdown. Humeral adduction gradually decreased through stance from an average of $-40°$ below the horizontal to $-20°$ at the end of stance, and then abducted to near horizontal (about $-8°$) during swing phase (Fig. 3). The humerus pronated rapidly at the beginning of stance phase from 10 to $-12°$, and then maintained a relatively constant level of pronation through midstance before rapidly supinating to $24°$ near the end of swing. As with protraction/retraction, pronation for the following stance phase began prior to foot contact. In addition to rotational degrees of freedom, the humeral head also slid posteriorly along the convexity of the glenoid an average of $18.6 \pm 7.6\%$ of the humeral head long-axis.

Near the end of stance, as the contralateral forelimb landed, a small increase in protraction, sliding and supination occurred in almost all strides, followed by a rapid slide/retraction and pronation through the end of toe off (Fig. 3).

Elbow joint

The elbow is formed by the articulation of the ulna and radius with the distal humerus. The lateral and medial distal condyles of the humerus form a shallow intercondylar pit into which a rounded process of the ulnar articular cartilage fits (Fig. 6a). An additional articular groove medial to the ulnar process articulates with the medial condyle of the humerus. The proximal radius articulates on the lateral condyle of the humerus and with the proximal ulna. These complex surfaces of the articular cartilages are not reflected in the underlying bones (Fujiwara, 2009; Holliday et al. 2010; Hutson, 2012).

The elbow was extended at manus down (about 130°), flexed to about 106° through mid-stance and re-extended to about 150° through late stance until toe off. During swing phase, the elbow flexed to an average of 90° and then extended prior to foot down through a total average range of $73 \pm 23°$.

The elbow was not a simple hinge; motion entailed both substantial abduction/adduction (mean range $41 \pm 10°$) and pronation/supination (mean range: $30 \pm 10°$; Table 2). In addition, the radius appeared to translate relative to the ulna, but no attempt was made to quantify this motion in

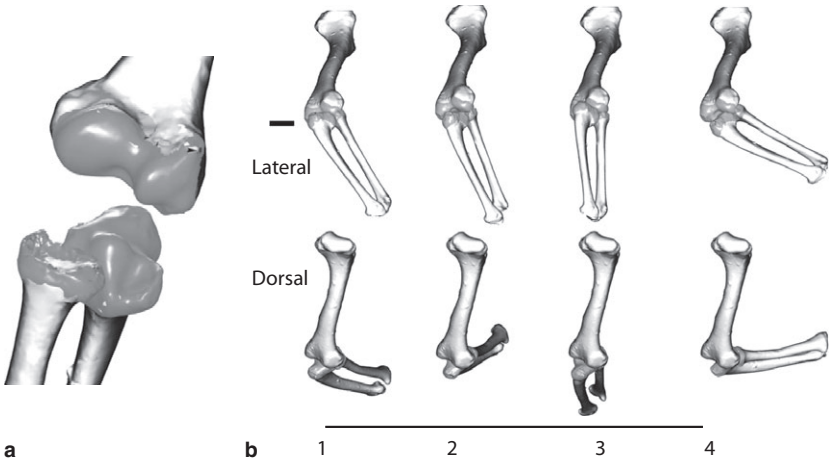

Fig. 6 Elbow joint. (a) The ulnar articular cartilage has a small peg-like bump that fits into a central pit on the humerus. The medial groove on the ulna articulates with the medial condyle and the lateral ulnar surface articulates with the radius. The radius articulates on the lateral condyle. (b) Motion of the elbow relative to the humerus during a single stride in lateral and dorsal view. 1 = forelimb down; 2 = mid-stance; 3 = late stance; 4 = late swing.

this study. The elbow abducted about 20° at peak flexion during stance phase and adducted about 20° during swing phase. At the beginning of stance phase, the pronated forearm gradually supinated through mid-stance, then pronated through late stance, and rapidly supinated after toe-off. In late swing, the humerus pronated again as the limb approached foot down (Fig. 3, 6b,c).

Hierarchical contributions to forelimb movement

During walking, the manus oscillates back and forth relative to the direction of travel in treadmill and vertebral reference frames (Gatesy & Baier, 2005). Manus displacement comes about through the coordinated motion of the hierarchical joint chain. We measured the relative contribution of four sources of manus excursion in the direction of travel during treadmill walking: (i) lateral undulations (yaw) of the vertebral column; (ii) the coracosternal joint; (iii) the glenohumeral joint; and (iv) the elbow joint.

Others have developed methods for assessing individual joint contributions to stride length (Fischer & Lehmann, 1998; Fischer et al. 2010). Here, we characterized each joint's contribution to forward motion by tracking the fore-aft displacement of the tip of the third distal phalanx (Fig. 7). We calculated individual joint contributions by negating each joints' movement, starting with the wrist/digital joints, followed by the elbow and then sequentially moving up the hierarchical chain. For each more proximal joint, the effects of all distal joints were removed by fixing them in their average pose over the complete stride (following Baier et al. 2013). For example, fixing the average position of the third phalanx position relative to the elbow effectively negates the effects of the wrist, metacarphalangeal and interphalangeal joints. Negating the hand joints reduced fore-aft translation of the manus $9.2 \pm 4\%$. The elbow accounted for $19 \pm 6\%$, the glenohumeral joint $24.2 \pm 5\%$, the coracosternal joint $30.5 \pm 3\%$ and body yaw (lateral undulation) contributes $16.7 \pm 3\%$.

Discussion

Skeletal kinematics – comparison to lizards

Lateral bending of the body during walking is typical for terrestrial lizards (Ritter, 1992) and crocodylians (Reilly & Elias, 1998; Carpenter, 2009). Reilly & Elias (1998) found that the patterns of body undulations were retained for alligators regardless of speed or gait. Lateral bending in the region of the shoulder girdles (yaw, about 21°) closely matched that of the terrestrial lizard *Agama* moving slowly (about 24°; Peterson, 1984), but was lower than that of *Varanus* (40–60°; Jenkins & Goslow, 1983). If correctly phased, yawing increases stride length by rotating the swing limb cranially and the stance limb caudally. Lateral undulations were reported to account for 24% of stride length in *Agama* (Peterson, 1984) compared with about 17% for alligators in this study. Hence, it would appear that crocodylians share the typical lepidosaurian pattern of lateral bending as a substantial component of stride length. In specialized arborealists, like *Chameleo*, lateral undulation is reduced, presumably to keep the center of mass over the branch (Fischer et al. 2010).

Coracosternal sliding in *Alligator* was found to be of considerable magnitude. Craniocaudal sliding at this joint has been hypothesized to increase step length in lizards (Gray, 1968). Jenkins & Goslow (1983) measured such motion in *Varanus* during walking. They characterized sliding as a displacement percentage relative to the total joint length of approximately 40%. Peterson (1984), however, found no evidence of coracosternal sliding in the terrestrial *Agama*, but significant coracosternal motion in the arboreal *Chameleo*. Because *Chameleo* did not employ lateral undulations on its narrow arboreal substrate, Peterson posited that coracosternal motion might be an arboreal adaptation to increase step length. Although Peterson's (1984) study relied on cinematography to infer coracosternal mobility, more recent 3-D skeletal analysis has confirmed coracoid

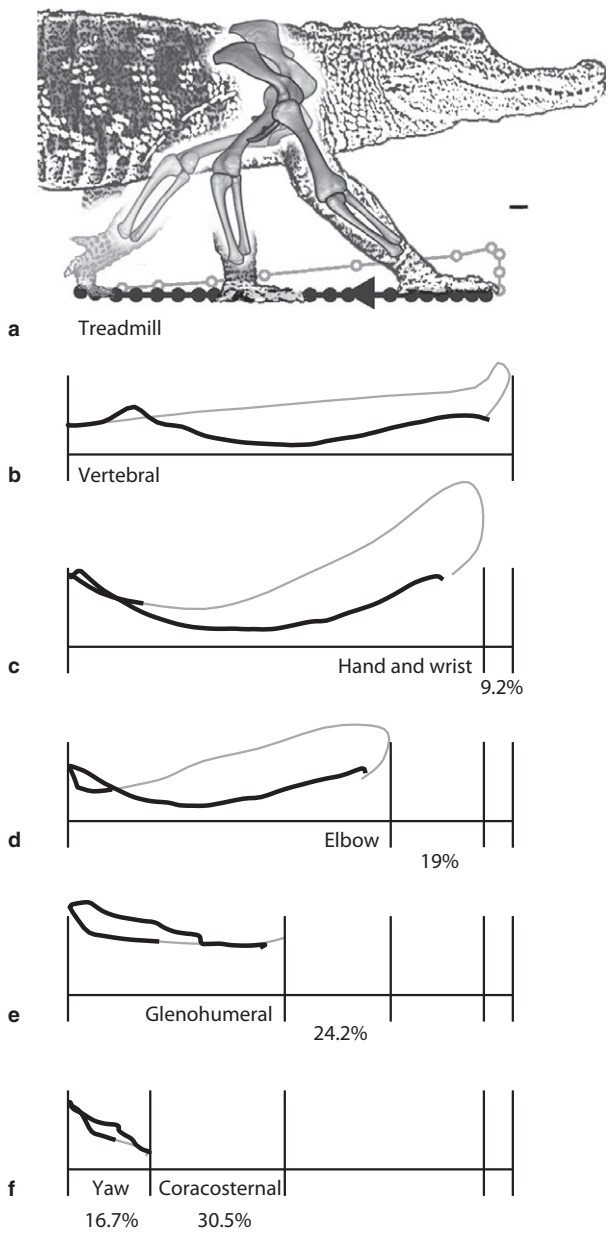

Fig. 7 Joint contributions to stride length. The tracings represent displacement of the fingertip during a single stride from Alligator1 after subtracting motion of each subsequent joint. The percentages represent the average contribution (20 strides; three animals) of each element to the fore-aft translation of the manus. (a) Treadmill reference frame. (b) Vertebral reference frame. (c) Hand and wrist motion account for 9.2% of stride length on average. (d) The elbow accounts for 19%. (e) The glenohumeral joint contributes 24.2%. (f) Coracosternal motion accounts for 30.5%. (g) The remaining stride length (16.7%) results from yaw of the body in the region of the shoulder girdle. Scale bar: 1 cm.

mobility for chameleons (Fischer et al. 2010). However, our findings do not support the hypothesis that coracoid mobility is purely an arboreal adaptation. A mobile coracoid may be an ancestral feature that is further expanded in arboreal lizards and further constrained in some terrestrial lizards. The basal condition of coracosternal mobility in diapsids, lepidosuars and archosaurs remains unresolved.

In this study, the cartilaginous sternum is not visible on the X-ray images, making it difficult to assess whether observed coracoid motion occurs only at the coracosternal joint or results from movement of the entire shoulder girdle (interclavicles + paired sterna). If asymmetric rib motions are significant during walking, it is possible that the interclavicle and paired sterna yaw as a unit relative to the vertebral column. However, the coracoid models could not be correctly positioned and oriented as a fixed pair, therefore indicating independent motion of the coracoids. Furthermore, lateral X-rays showed no movement of the interclavicle relative to the dorsal markers (suggesting, at least, no anterior/posterior translation or pitching rotation). Yet, it is still possible that some combination of coracosternal movement and bilateral shoulder girdle/thoracic movement contribute to the observed pattern of movement between the coracoids and dorsal markers. More studies are needed to address this possibility.

The change from caudal to cranial sliding, however, does not occur at the beginning of swing phase. Instead, the coracoid begins to slide forward either at or near the time that the ipsilateral hindlimb contacts the tread in late stance. The two smaller alligators tended to have larger amounts of coracoid sliding (71.7% of coracoid width) compared with Alligator1 (46.8%).

Alligator coracosternal sliding averaged 50% of the total joint length, and coracoid movements account for 30% of the displacement of the manus during a stride. Hence, like *Varanus*, both lateral body undulations and coracoid motion play a sizeable role in forelimb excursion. This supports the hypothesis that coracosternal sliding is primitive for diapsids (Gray, 1968). If *Agama* truly lacks coracosternal sliding, it is possible that coracosternal sliding is a derived condition for this group, calling into question the adaptive significance of a fixed coracosternal joint in terrestrial saurians. Hence, the basal function of the coracosternal joint in both diapsids and archosaurs remains ambiguous.

The ranges of *Alligator* humeral protraction/retraction (57.7°) and pronation/supination (39°) were similar to *Varanus* (40–55° and 30–40°, respectively; Jenkins & Goslow, 1983). However, *Alligator* humeral abduction/adduction ranged from 48° below the horizontal to 8° above the horizontal compared with 10° below the horizontal and 35° above the horizontal for *Varanus*, reflecting the difference between the high-walk of the alligator and the sprawling walk of lizards.

Jenkins & Goslow (1983) did not quantify glenoid sliding in *Varanus*, but it was later suggested to play a role in facilitating humeral protraction/retraction (Jenkins, 1993). Glenoid sliding averaged 2.7 mm along the articular surface or 18% of the long-axis width of the humeral head in *Alligator*. Although this does increase the anteroposterior excursion of

the limb slightly, its impact is minor. This calls into question the hypothesis that humeral head translation primarily functions to magnify the effect of protraction/retraction. It may instead be a consequence of the elongate bulbous head of the humerus. It may be that the translational movement provided by the elongate humeral head allows soft tissues spanning the joint to maintain a more effective lever arm through the stride. An additional possibility is that pronation/supination are constrained by the scapular and coracoidal lips of the glenoid under certain loading conditions, which would require that the humeral head be longer than the glenoid. Further investigation into the magnitude and effect of glenoid sliding and the mechanics of the joint are needed to address these possibilities.

The major patterns of body motion and skeletal kinematics affecting shoulder movement are very similar between crocodylians and lepidosaurs, despite the differences in morphology of the shoulder girdle and the more semi-erect posture used during the high-walk. Hence, it appears that many forelimb locomotor features (yaw of the body in the shoulder region, coracosternal sliding and glenohumeral motions) are ancestral features for Archosauria.

Comparison to birds

The kinematic patterns of flapping in birds and walking in alligators can be homologized relative to a glenoid reference frame (Jenkins, 1993; Gatesy & Baier, 2005). Crocodylian protraction/retraction equates with elevation/depression in birds, and crocodylian abduction/adduction matches with avian protraction/retraction. Jenkins (1993) found that the avian humeral head not only rotates, but that the long-axis of the humeral head also translates along the convexity of the glenoid. This presumably increases the range of motion in the primary plane of wing movement. These same four degrees of freedom were found to operate at the shoulder joint of *Alligator*, confirming that the glenoid reference frame is comparable between the two, despite the 90° difference in glenoid orientation relative to the vertebral column (Gatesy & Baier, 2005).

Several intriguing differences arise when comparing the shoulder kinematics between these clades. First, yaw of the body and large coracosternal translations impart almost half of the anterior/posterior displacement of the wrist in walking alligators. Yawing is only effective because the contralateral limbs operate out of phase. The synchronous forelimb motions in flapping birds negate the potential to increase the limb excursion through body undulations. Either coracosternal or glenohumeral motion must play a larger relative role in limb excursion during flapping. Coracosternal motions do occur in avian species with flexible wishbones (Jenkins et al. 1988; Baier et al. 2013), but the magnitude of this effect on wing excursion has not been quantified. Further comparisons between extant archosaur coracosternal joints are warranted.

Our findings reveal a major question in the evolution of the archosaur shoulder joint: if bird wings have lost effects of body yaw and coracosternal motions (which account for about 47% of *Alligator* stride length), how do they maintain large wing excursions? The glenohumeral joint would have to provide a much larger contribution to the overall excursion of the wing. Glenohumeral elevation/depression in starlings (flying between 10 and 16 m s^{-1}) ranges about 80° (*Sturnus vulgaris*; Dial et al. 1991) after converting their measurement system to the one used in this study. This compares to a range of 52–62° for the *Alligator* about the homologous protraction/retraction axis. Despite the similarities in the glenoid, there may be major differences in the range of motion used during flapping and walking. What morphological features affect this difference in glenohumeral excursion? Are they differences in the range of motion used or differences in the range of motion available? Detailed comparative analyses of skeletal kinematics for multiple species and multiple speeds are needed to address these questions.

Conclusions

Three-dimensional reconstructions of skeletal motion using X-ray video of alligators reveal considerable coracoid movements during high-walks. The importance of shoulder girdle contributions to locomotion are well known in mammals (Jenkins & Weijs, 1979), but less thoroughly explored in diapsids and archosaurs. This study brings to light new questions regarding the basal condition and evolutionary trends of shoulder girdle mobility within these groups. Future investigations of other taxa and more detailed analyses of the movements in alligators are needed to clarify the evolutionary significance of either permitting or restricting movements of shoulder girdle elements.

Acknowledgements

The authors are grateful to F. Jenkins Jr and A. Crompton for lending access to equipment and assistance in the X-ray facilities at Harvard. The authors also thank C. Sullivan and L. Claessens for sharing alligator video and specimens. Autodesk are thanked for the use of Maya software, and the SHAPE lab at Brown University are thanked for providing access to 3-D laser-scanning equipment (NSF/ITR grant #0205477). In particular, P. Bazin, F. Leymarie and A. Willis are acknowledged for extensive time and effort in laser-scanner training. Also, thanks to Brigid Garrity for helping revise the developing manuscript.

References

Allen V, Elsey RM, Jones N, et al. (2010) Functional specialization and ontogenetic scaling of limb anatomy in *Alligator mississippiensis*. *J Anat* **216**, 423–445.

Baier DB, Gatesy SM, Dial KP (2013) Three-dimensional, high-resolution skeletal kinematics of the avian wing and shoulder

during ascending flapping flight and uphill flap-running. *PLoS ONE* **8**, e63982.

Bakker RT (1971) Dinosaur physiology and the origin of mammals. *Evolution* **25**, 636–658.

Blob RW, Biewener AA (1999) *In vivo* locomotor strain in the hindlimb bones of *Alligator mississippiensis* and *Iguana iguana*: implications for the evolution of limb bone safety factor and non-sprawling limb posture. *J Exp Biol* **202**, 1023–1046.

Blob RW, Biewener AA (2001) Mechanics of limb bone loading during terrestrial locomotion in the green iguana (*Iguana iguana*) and American alligator (*Alligator mississippiensis*). *J Exp Biol* **204**, 1099–1122.

Brainerd EL, Baier DB, Gatesy SM, et al. (2010) X-ray reconstruction of moving morphology (XROMM): precision, accuracy and applications in comparative biomechanics research. *J Exp Zool A Ecol Genet Physiol* **313A**, 262–279.

Carpenter K (2009) Role of lateral body bending in crocodylian track making. *Ichnos* **16**, 202–207.

Cott HB (1961) Scientific results of an inquiry into the ecology and economic status of the Nile Crocodile, *Crocodylus niloticus*, in Uganda and northern Rhodesia. *Trans Zool Soc London* **29**, 211–337.

Dial KP, Goslow GEJ, Jenkins FA (1991) The functional anatomy of the shoulder in the European Starling (*Sturnus vulgaris*). *J Morphol* **207**, 327–344.

Dobbert T (2005) *Matchmoving: The Invisible art of Camera Tracking*. Alameda, CA: Sybex.

Fischer MS, Lehmann R (1998) Application of cineradiography for the metric and kinematic study of in-phase gaits during locomotion of the pika (Ochotona rufescens, Mammalia: Lagomorpha). *Zoology* **101**, 148–173.

Fischer MS, Krause C, Lilje KE (2010) Evolution of chameleon locomotion, or how to become arboreal as a reptile. *Zoology* **113**, 67–74.

Fujiwara S-i (2009) Olecranon orientation as an indicator of elbow joint angle in the stance phase, and estimation of forelimb posture in extinct quadruped animals. *J Morphol* **270**, 1107–1121.

Gatesy SM (1991) Hind limb movements of the American alligator (*Alligator mississippiensis*) and postural grades. *J Zool Lond* **1991**, 577–588.

Gatesy SM (1997) An electromyographic analysis of hindlimb function in alligator during terrestrial locomotion. *J Morphol* **234**, 197–212.

Gatesy SM, Baier DB (2005) The origin of the avian flight stroke: a kinematic and kinetic perspective. *Paleobiology* **31**, 382–399.

Gatesy SM, Baier DB, Jenkins FA, et al. (2010) Scientific rotoscoping: a morphology-based method of 3-D motion analysis and visualization. *J Exp Zool A Ecol Genet Physiol* **313A**, 244–261.

Gray SJ (1968) *Animal Locomotion*. London: Weidenfeld and Nicolson.

Grood ES, Suntay WJ (1983) A joint coordinate system for the clinical description of three-dimensional motions: application to the knee. *J Biomech Eng* **105**, 136–144.

Holliday CM, Ridgely RC, Sedlmayr JC, et al. (2010) Cartilaginous epiphyses in extant archosaurs and their implications for reconstructing limb function in dinosaurs. *PLoS ONE* **5**, e13120.

Hutchinson JR (2006) The evolution of locomotion in archosaurs. *CR Palevol* **5**, 519–530.

Hutson JD (2012) A test of the validity of range of motion studies of fossil archosaur elbow mobility using repeated-measures analysis and the extant phylogenetic bracket. *J Environ Biol* **215**, 2030.

Hutson JD, Hutson KN (2012) Using the American alligator and a repeated-measures design to place constraints on *in vivo* shoulder joint range of motion in dinosaurs and other fossil archosaurs. *J Exp Biol*, **216**, 275–284.

Jasinoski SC, Russell AP, Currie PJ (2006) An integrative phylogenetic and extrapolatory approach to the reconstruction of dromaeosaur (Theropoda: Eumaniraptora) shoulder musculature. *Zool J Linn Soc* **146**, 301–344.

Jenkins FAJ (1993) The evolution of the avian shoulder joint. *Am J Sci*, **293-a**, 253–267.

Jenkins FA, Goslow GEJ (1983) The functional anatomy of the shoulder of the Savannah monitor lizard (*Varanus exanthematicus*). *J Morphol* **175**, 195–216.

Jenkins FAJ, Weijs WA (1979) The functional anatomy of the shoulder in the Virginia opossum (*Didelphis virginiana*). *J Zool* **188**, 379–410.

Jenkins FA, Dial KP, Goslow GEJ (1988) A cineradiographic analysis of bird flight: the wishbone in starlings is a spring. *Science* **241**, 1495–1498.

Leardini A, Chiari L, Croce UD, et al. (2005) Human movement analysis using stereophotogrammetry: part 3. Soft tissue artifact assessment and compensation. *Gait Posture* **21**, 212–225.

Meers MB (2003) Crocodylian forelimb musculature and its relevance to archosauria. *Anat Rec A Discov Mol Cell Evol Biol* **27A**, 891–916.

Nesbitt SJ (2011) The early evolution of archosaurs: relationships and the origin of major clades. *Bull Am Mus Nat Hist* **352**, 1–292.

Nicholls EL, Russell AP (1985) Structure and function of the pectoral girdle and forelimb of *Struthiomimus altus* (Theropoda: Ornithomimidae). *Palaeontology* **28**, 643–677.

Nyakatura JA, Fischer MS (2010) Three-dimensional kinematic analysis of the pectoral girdle during upside-down locomotion of two-toed sloths (*Choloepus didactylus*, Linné 1758). *Front Zool* **7**, 1–21.

Paul GS, Christiansen P (2000) Forelimb posture in neoceratopsian dinosaurs: implications for gait and locomotion. *Paleobiology* **26**, 450–465.

Peterson JA (1984) The locomotion of *Chamaeleo* (Reptialia: Sauria) with particular reference to the forelimb. *J Zool Lond* **202**, 1–42.

Reilly SM, Blob RW (2003) Motor control of locomotor hindlimb posture in the American alligator (*Alligator mississippiensis*). *J Exp Biol* **206**, 4327–4340.

Reilly SM, Elias JA (1998) Locomotion in *Alligator mississippiensis*: kinematic effects of speed and posture and their relevance to the sprawling-to-erect paradigm. *J Exp Biol* **201**, 2559–2574.

Reilly SA, Willey JS, Biknevicius AR, et al. (2005) Hindlimb function in the alligator: integrating movements, motor patterns, ground reaction forces and bone strain of terrestrial locomotion. *J Exp Biol* **208**, 993–1009.

Renous S, Gasc JP, Bels VL, et al. (2002) Asymmetrical gaits of juvenile Crocodylus johnstoni, galloping Australian crocodiles. *J Zool* **256**, 311–325.

Ritter D (1992) Lateral bending during lizard locomotion. *J Exp Biol* **173**, 1–10.

Willey JS, Biknevicius AR, Reilly SM, et al. (2004) The tale of the tail: limb function and locomotor mechanics in *Alligator mississippiensis*. *J Exp Biol* **207**, 553–563.

Witmer L (1995) Homology of facial structures in extant archosaurs (birds and crocodilians), with special reference to para-

nasal pneumaticity and nasal conchae. *J Morphol* **225**, 269–327.

Zatsiorsky VM (1998) *Kinematics of Human Motion*. Champaign, IL: Human Kinetics.

Zug GR (1974) Crocodilian galloping: an unique gait for reptiles. *Copeia* **2**, 550–552.

Supporting Information

Additional Supporting Information may be found in the online version of this article:

Video S1. Rotoscoping Method. This video documents the process of reconstructing 3-D skeletal motion.